Electronic structure in icosahedral AlCuLi quasicrystals and approximant crystals

1994 J. Phys.: Condens. Matter 6 6977

(http://iopscience.iop.org/0953-8984/6/35/008)

J. Phys.: Condens. Matter 6 (1994) 6977–6995. Printed in the UK

Electronic structure in icosahedral AlCuLi quasicrystals and approximant crystals

M Windisch, M Krajčí† and J Hafner
Institut für Theoretische Physik, TU Wien, Wiedner Hauptstraße 8-10, A-1040 Wien, Austria

Received 13 April 1994, in final form 2 June 1994

Abstract. The electronic structure has been calculated for large approximant crystals (up to 51 752 atoms in the periodically repeated cell) to icosahedral AlCuLi quasicrystals. The results show that a deep structure-induced pseudogap at the Fermi energy is a generic property of the quasicrystal and its crystalline approximants. The physical mechanism for the formation of the gap is discussed on the basis of a quasiperiodic generalization of the nearly-free-electron model.

1. Introduction

Since the discovery of quasicrystals [1], the problem of why and under what circumstances nature prefers quasiperiodic to periodic order has received much attention. There have been early suggestions [2–6], based largely on electron-counting arguments, that the energetic stability is promoted by a Hume–Rothery-like mechanism, leading to the formation of a pseudogap in the electronic density of states at the Fermi level. On the experimental side, this argument is supported by the discovery [7–9] that the electronic properties of stable quasicrystals such as Al_7Pd_2Mn, Al_7Cu_2Fe or Al_6Li_3Cu exhibit striking semimetallic properties, with low-temperature electronic resistivities orders of magnitude larger than those found in ternary amorphous alloys [10]. Quite generally, the more stable and more perfect the quasicrystal (as measured by the grain size), the larger the low-temperature resistivity ρ_0, the more negative the temperature coefficient $(1/\rho)(d\rho/dT)$ of the resistivity, and the lower the electronic density of states $n(E_F)$ at the Fermi level [11]. However, the existence of a structurally induced pseudogap at E_F alone is not sufficient evidence for a predominantly electronic mechanism promoting quasicystalline stability: structure-induced gaps or pseudogaps exist also in certain metallic glasses [12–15], in the crystalline Hume–Rothery compounds [16, 17] and in a certain class of crystalline compounds that are found at compositions close to that of the quasicrystalline phase [18–20], e.g. α-AlMnSi, R-AlCuLi and $(Al,Zn)_{49}Mg_{32}$. The atomic arrangement in these crystals is believed to be similar to the local order in the quasicrystal. The lattice of these approximant crystals may be specified by the rational number $\tau_n = F_{n+1}/F_n$ approximating the irrational number $\tau = (1 + \sqrt{5})/2$ (the golden mean) defining the incommensurability of the quasicrystal. The α-AlMnSi, R-AlCuLi and $(Al,Zn)_{49}Mg_{32}$ phases are the 1/1-approximants to the corresponding quasicrystals, and in some cases higher-order approximants (e.g. a 3/2-approximant [21] to icosahedral AlZnMg) exist. Hence the question arises whether the quasicrystal receives more band-gap stabilization than the competing crystalline and amorphous phases.

† Permanent address: Institute of Physics, Slovak Academy of Sciences, SK-84228 Bratislava, Slovakia.

0953-8984/94/356977+19$19.50

There have been many experiments to demonstrate the existence of a pseudogap in quasicrystalline alloys by various spectroscopic techniques [22–25], but only a very few studies [26, 27] have succeeded in demonstrating that the pseudogap is slightly more pronounced in the quasicrystal than in the approximant phase—a notable example is just the icosahedral AlCuLi phase. The experiments are hampered by the fact that the properties of the quasicrystal depend often quite sensitively on the preparation of the specimen [28].

Under these circumstances, theoretical predictions of the electronic properties of quasicrystals are highly desirable. The problem is that standard techniques for electronic structure calculations based on the use of Bloch's theorem are applicable only to systems with a maximum of a few hundred atoms per unit cell. For this reason, most electronic structure calculations refer to the lowest-order approximants: R-AlCuLi [29], α-AlMnSi [30], $(Al,Zn)_{49}Mg_{32}$ [31]—all 1/1-approximants to the icosahedral phases. Larger systems may be treated using approximate techniques working in real space, such as the recursion technique. To date, electronic structure calculations for realistic higher-order approximants have been presented only for AlZnMg (up to the 5/3-approximants with 12 380 atoms in the periodic cell) [32–34]. In this system, the pseudogap shows no systematic variation in the hierarchy of the approximants. This is not surprising, since the 3/2-approximant as well as the icosahedral quasicrystal exist only as metastable phases. It is therefore compelling to extend the investigations to stable quasicrystals. The problem is that these calculations must be performed for accurate structural models. For the icosahedral AlZnMg phase such a model [35] is given by a three-dimensional Penrose tiling, with a decoration proposed by Henley and Elser [36] (derived from the structure of the $(Al,Zn)_{49}Mg_{32}$ Frank–Kasper phase [18]). For AlCuLi, the applicability of the Henley–Elser model has been disputed [37]. Only very recently we have been able to show [38] that a slightly modified Henley–Elser model describes the structure of icosahedral AlCuLi very accurately and may be reconciled with alternative descriptions of the quasicrystalline lattice based on canonical cell tiling concepts [39, 40] or the decoration of large (τ^3-inflated) Penrose (or Ammann) rhombohedra with icosahedral clusters [37, 41].

In the present paper, we present a systematic study of the electronic structure of a hierarchy of rational approximants to icosahedral AlCuLi—up to 8/5-approximants with more than 5×10^4 atoms in the periodically repeated unit. The calculations are based on a self-consistent linear-muffin-tin orbital (LMTO) technique [42] for the 1/1-approximant and on tight-binding LMTO calculations [43, 44] performed with recursion techniques [45] for the higher-order approximants. The paper is organized as follows: In section 2 we review very briefly the geometrical properties of the approximant structures, section 3 summarizes the technical aspects of the TB-LMTO recursion technique. The variation of the electronic density of states (DOS) in the hierarchy of the approximants and its dependence on the details of the structural model is discussed in section 4. In section 5 we describe the Bloch spectral functions of electrons in a large approximant and derive the dispersion relations of electrons in a repeated Brillouin-zone scheme of the approximant (corresponding to a scheme of quasiperiodic Brillouin zones in the infinite limit). This helps to elucidate the origin of the structure-induced electronic pseudogap at the Fermi level. In section 6 we discuss very briefly the photoelectron- and soft x-ray spectra and compare with the available sprectroscopic data. In section 7 we present our conclusions.

2. Atomic structure

Attempts to model the structure of i-AlCuLi have been made on the basis of: (a) three-dimensional Penrose tilings decorated with atoms [35, 38], (b) τ^3-inflated Penrose tilings

decorated with icosahedral clusters [46], (c) canonical cell tilings [38–40], again decorated with large icosahedral clusters and (d) direct projections from six-dimensional space, with atomic surfaces determined on the basis of the six-dimensional Patterson functions [41]. A comparative discussion of these models and details of their construction are given in [38]; in the following we recapitulate only those aspects of the construction of the approximants that are of immediate relevance for the discussion of the electronic structure.

2.1. Three-dimensional periodic Penrose tiling

The three-dimensional Penrose tiling (3DPT) has been proposed as one of the earliest models for quasiperiodic lattices [47]. For the quasicrystals of the i-AlZnMg and i-AlCuLi classes, an atomic decoration of the Penrose rhombohedra with atoms has been proposed by Henley and Elser [19] on the basis $(Al,Zn)_{49}Mg_{32}$ Frank–Kasper phase and the R-phase Al_6CuLi_3. The two classes of structures differ only in the occupation of the twelvefold vertices of the lattices which are occupied for i-AlZnMg, but remain vacant in i- and R-phase AlCuLi.

The lowest-order approximant is built by multi-shell triacontahedra of 136 atoms centred on the twelvefold vertices, touching and interconnected with other triacontahedra. The symmetry of the 1/1-approximant is body-centred cubic, space group Im3. Although the elemental Penrose rhombohedra are decorated in the same way in all approximants, the large triacontrahedral clusters do not necessarily remain intact in the higher-order approximants.

The rational approximant is not entirely determined by specifying the rational approximation τ_n to τ. In addition, there is the possibility of shifting the triacontahedral acceptance domain in perpendicular space over a range that shrinks with increasing n. This degree of freedom is related to a phason mode—a shift of the acceptance domain changes the spatial arrangement of the Penrose tiles, but not their frequency. To illustrate the effect of such a rearrangement on the electronic structure, we have considered two variants of the 1/1-approximant: one with the position of the acceptance domain leading to the R-phase and one with a shifted acceptance domain (in a centrosymmetric position) leading to a high-symmetry crystalline approximant (space group $I2_13$, a full crystallographic description of similar variants of low-order approximants is given in [35]).

2.2. Canonical cell tiling

The building principle of the canonical cell tiling introduced by Henley [39] is to fill space with four types of 'canonical cells': a distorted ('BCC') tetrahedron, half a trigonal antiprism, a triangular pyramid and a trigonal prism. The cells can be decorated with Penrose rhombohedra without gaps and overlaps, and this decoration defines a set of packing rules for the cells. The motivation for the introduction of the canonical cell tiling (CCT) concept was twofold: (a) to build an icosahedral network of the inter-cluster linkages existing between the triacontahedral clusters in the R-phase (b-bonds along cube edges and c-bonds along half the body diagonal), and (b) to optimize the density of the b–c network.

A central problem of the CCT concept is that the proof of quasiperiodicity is still lacking. However, Newman and Henley [48] have developed a transfer-matrix technique which explicitly generates all approximants up to 5/3, and Mihalkovič and Mrafko [40, 49] have developed a technique based on a Monte Carlo optimization of the b–c network and applied it to the generation of CCTs up to the 13/8-approximant.

A detailed discussion of the application of the CCT concept to i-AlCuLi and of the relation of the CCT and 3DPT models is given in [48, 49]. With the position of the acceptance domain leading to the R-phase structure, the 1/1-, 2/1- and 3/2-approximants are identical in the CCT and 3DPT schemes. Differences appear in the higher-order approximants, where

the CCT models preserve the integrity of the 136-atom triacontahedral clusters (placed on the twelvefold nodes of the CCT) whereas the 3DPT models do not.

The integrity of the 136-atom clusters is a feature that the CCT shares with the cluster-decoration models of the τ^3-inflated Penrose tilings. However, as the CCT maximizes the density of the b–c network, it also minimizes the number of glue atoms (i.e. of atoms that do not belong to any of the triacontahedral clusters) to about 2% even in the largest approximants (to be compared with at least 20% glue atoms in the cluster tiling models).

2.3. Displacive modulation

In a quasicrystal or in a higher-order approximant any atom is found in a very large number of different environments. Hence the interatomic forces will lead to a displacive modulation of the idealized model: if the structure is stable, the displacement field will have the same symmetry as the idealized lattice. We have determined the displacement field by molecular dynamics annealing and conjugate-gradient optimization of the equilibrium positions under realistic interatomic forces (see [38] for details). Both the 3DPT and the CCT models are stable up to the 8/5-approximant (the largest model included in our study). At the level of partial pair-correlation functions of the relaxed structures, the CCT and 3DPT models are virtually indistinguishable and in very good agreement with experiment. The same applies to the powder-diffraction spectra. Minor differences appear in the single-crystal diffraction data, where a slight preference for the CCT models appears. For later use we present in figure 1 the intensities of the Bragg peaks in a plane containing the two-, three- and five-fold symmetry axis, calculated for the 5/3-approximant to the 3DPT (the CCT model gives an essentially undistinguishable result).

3. Calculation of the electronic structure

For the 1/1-approximant with a 160-atom cubic cell, the electronic structure has been calculated self-consistently, using the standard LMTO technique [42] in the atomic-sphere approximation (ASA). Brillouin-zone integrations have been performed using the linear tetrahedron technique, based on a grid of 55 k-points in the irreducible part of the zone.

For the higher-order approximants, the LMTO Hamiltonian is transformed to a tight-binding (TB) form. The two-centre TB Hamiltonian in the Löwdin orthogonal representation is given by [43, 44] (a superscript γ defines quantities calculated in a nearly orthogonal basis)

$$H^\gamma = \epsilon_\nu + h^\gamma \tag{1}$$

where ϵ_ν ($\nu = nlm$) is the reference energy for the linearization of the MTOs. The Hamiltonian (1) is accurate to second order in $(E - \epsilon_\nu)$. The matrix h^γ is determined by the expansion

$$h^\gamma = h^\alpha + h^\alpha o^\alpha h^\alpha + h^\alpha o^\alpha h^\alpha o^\alpha h^\alpha \ldots \tag{2}$$

where h^α and o^α are the Hamiltonian and overlap matrices in a screened, most localized basis. h^α satisfies the relation

$$H^\alpha = \epsilon_\nu + h^\alpha = c^\alpha + \sqrt{d^\alpha}\, S^\alpha \sqrt{d^\alpha} \tag{3}$$

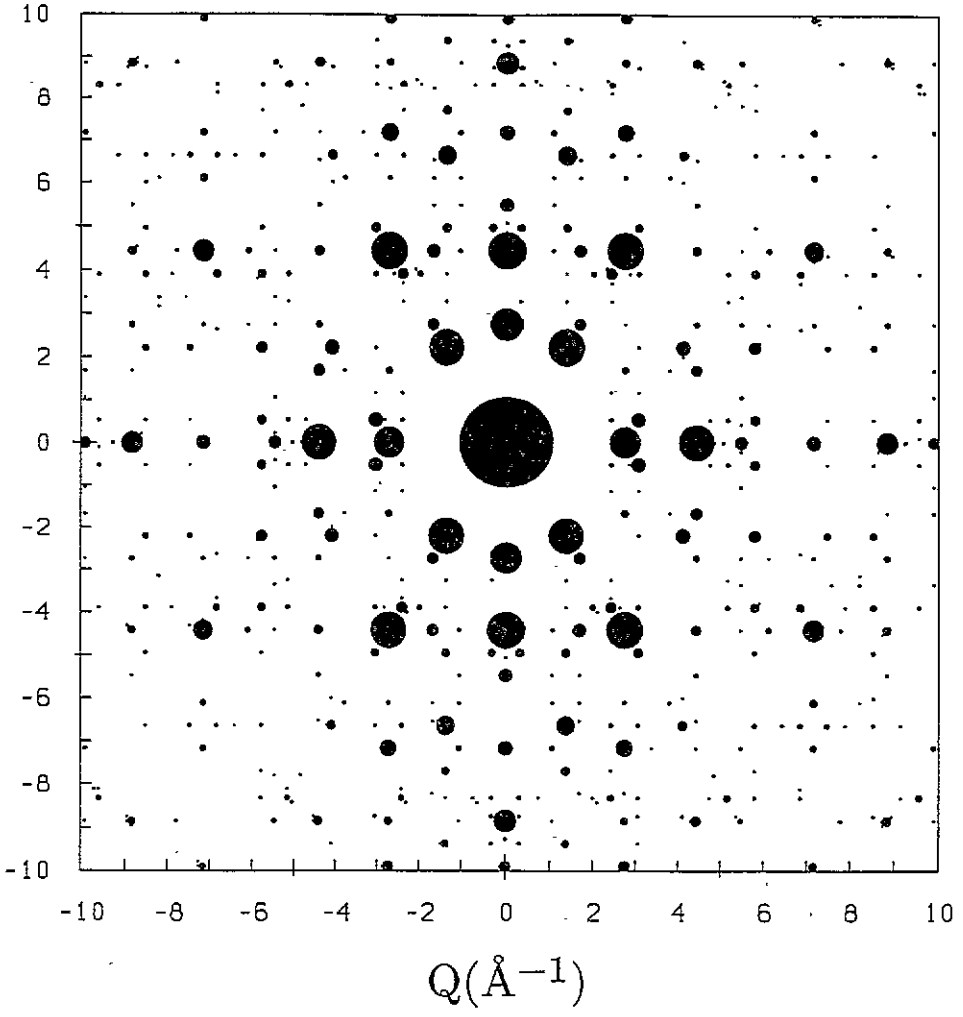

Figure 1. Distribution and intensities of Bragg peaks in a plan containing the two-, three- and five-fold symmetry axes, calculated for the 5/3-approximant to the 3DPT model for i-AlCuLi.

where c^α and d^α are the diagonal matrices of the potential parameters describing the centre of gravity and the width of each band. S^α is the matrix of the screened structure constants

$$S^\alpha = S^0(1-\alpha S^0)^{-1} \tag{4}$$

calculated in terms of the standard LMTO structure constants S^0 and the diagonal screening matrix α with parameters $\alpha = (0.34848,\ 0.053030,\ 0.010714)$ for s, p and d orbitals, respectively [43]. When the standard LMTO potential parameters $C \equiv c^\gamma$, $\Delta \equiv d^\gamma$ and γ (standing for the asymmetry of the band) are known (we take them from the LMTO-ASA calculation for the 1/1-approximant), the screened potential parameters c^α, d^α and the overlap parameter o^α are obtained using the expression [43, 44]

$$\frac{c^\alpha-\epsilon_\nu}{c^\gamma-\epsilon_\nu}=\left(\frac{d^\alpha}{d^\gamma}\right)^{1/2}=\frac{\alpha-\gamma}{o^\alpha d^\gamma}=1+\frac{\alpha-\gamma}{d^\gamma}(c^\gamma-\epsilon^\gamma)\,. \tag{5}$$

The recursion method [45] is a real-space technique for calculating a projected density of states (DOS)

$$n_\psi(E) = -\frac{1}{\pi}\mathrm{Im}\langle\psi|(E + \mathrm{i}0^+ - H)^{-1}|\psi\rangle \tag{6}$$

in the form of a continued fraction expansion. If the initial state $|\psi\rangle$ is a local atomic orbital with quantum numbers nlm at the site R_i , the projected density of states is just the local partial DOS $n_{i,nlm}(E)$. If the initial state $|\psi\rangle$ is a Bloch function with wave vector k, the resulting projected DOS is the Bloch spectral function $f(k, E)$ of the electrons. The total DOS may be computed in three different ways. (a) By taking the average over the local DOS calculated on a large number of sites. This approach has the disadvantage that for an amorphous system it converges rather slowly. (b) By integrating the Bloch spectral functions $f(k, E)$ over a large volume in k-space. Again this approach is rather cumbersome, because it requires the calculation of $f(k, E)$ for many different k-vectors. (c) The most convenient way to produce the total DOS is to choose an initial state given in a TB basis as a vector $u_0^{\nu,R}$

$$u_0^{\nu,R} \sim \exp(\mathrm{i}\delta_{\nu,R})$$

where the $\delta_{\nu,R}$ are uniformly distributed random numbers in the interval $[0, 2\pi)$. This approach corresponds to taking an incoherent average over the local densities of state, as for a sufficiently large model interference effects cancel out. A possible statistical error resulting from the random sampling may be minimized by taking an average over several random vectors. A detailed comparative study of the three approaches has been given by Hafner [50].

Technically, the recursion method defines a basis in which the symmetric matrix H assumes a tridiagonal form. The inversion of $(E - H)^{-1}$ leads directly to the continuous fraction representation of the DOS. The continued fraction may be terminated at a level L that is much smaller than the dimension N of the Hamiltonian matrix. The information contained in the first L recursion coefficients is equivalent to that contained in $2 \times L$ moments of the DOS. For the largest approximant we used up to $L = 80$ recursion steps and obtained a smooth spectrum by applying a proper termination procedure (we used Gaussian quadrature [51] for the total DOS and the Lucchini–Nex terminator [52] for the Bloch spectral function).

4. Electronic density of states

4.1. 1/1-approximants

Figures 2(*a*), (*b*) show the total and the site- and angular-momentum-decomposed partial *electronic densities of states of R-phase* AlCuLi (i.e. the 1/1-approximant to the icosahedral phase with 160 atoms in the simple cubic cell) as obtained from a self-consistent LMTO calculation. The Brillouin-zone integration has been performed on a grid of 55 k-points in the irreducible wedge of the simple cubic Brillouin zone. Given the smallness of the Brillouin zone and the rather extended grid of k vectors, even the fine details of the spiky DOS are fully converged. The width of the band is almost equal to the free-electron bandwidth. The most prominent features of the DOS are the main peak at ~ 3 eV below the Fermi edge and the broad depression of the DOS around E_F. At the Fermi level, the DOS is $n(E_F) = 0.21$ states (eV atom)$^{-1}$; it drops to $n(E_F) \sim 0.13$ states (eV atom)$^{-1}$ only 0.03 eV below E_F.

This corresponds to about one-third of the free-electron DOS of $n_{fe}(E_F) \simeq 0.33$ states (eV atom)$^{-1}$. Experimental estimates from low-temperature heat-capacity measurements yield $n(E_F) = 0.13$ states(eV atom)$^{-1}$ [28]. The DOS minimum is most pronounced in the partial Al DOS, whereas the Al and Li contributions are already quite small at E_F. Figure 2(*b*) shows the decomposition of the local DOS into the s, p, d angular-momentum contributions. We find that the Al-s states are concentrated in the lower part of the band, whereas the states close to the Fermi level are predominantly of p character. A similar result holds for the Li states. The Cu states are predominantly d states.

Our results are in good agreement with earlier calculations of Fujiwara and Yokokawa [29, 53], except for a distinctly larger bandwidth in Fujiwara's calculation. This difference is due to two factors: we have allowed a random distribution of the Al (Cu) atoms over the available vertex and mid-edge positions in the ratio of Al:Cu = 46:8 ('G' positions inside the rhombic dodecahedron are only decorated by Al), although this breaks the BCC point-group symmetry. Fujiwara and Yokokawa tested different distributions of Al and Cu atoms compatible with the SC symmetry (leading to somewhat different stoichiometries).

Our configuration was relaxed under the constraint of conserving the symmetry. This allows us to eliminate unrealistically short interatomic distances that lead to strongly bound states below the bottom of the free-electron band.

The DOS minimum of the Fermi level is structure induced (the precise mechanism for the formation of the gap will be discussed below). Within a given class of approximants, the existence of the 'pseudogap' depends on the precise arrangement of the Penrose rhombohedra within the periodically repeated cell. This is demonstrated by a calculation for a high-symmetry 1/1-approximant with the acceptance domain shifted to a body-centred position within the allowed domain (see [35] for a more detailed discussion; the R-phase is obtained when the centre of the acceptance domain is placed at the origin). This symmetric 1/1-structure lacks the characteristic pseudogap of the R-phase, there is only a very slight depression in the DOS just below E_F (figure 3). The 1/1-approximant is the only one for which an electronic structure calculation with a conventional k-space technique such as the LMTO is computationally feasible, as already for the 2/1-approximant with 136 rhombohedra (and nearly 700 atoms) the computational effort associated with the standard technique is too large. The alternative is to use the real-space recursion technique, with a TB-LMTO Hamiltonian based on the self-consistent potentials.

Figure 4 compares the two results for the 1/1-approximant. We find that the recursion calculation reproduces all the main aspects of the electronic spectrum very well, but the necessary truncation of the continued fraction at a finite level leads to a smearing of the fine structure in the DOS. The DOS at E_F is $n(E_F)$=0.22 states (eV atom)$^{-1}$, the minimum at the DOS is $n(E)$=0.20 states (eV atom)$^{-1}$. This broadening means that the recursion calculations are sufficiently accurate to discuss any features of the electronic spectrum that could possibly be related to a spectroscopic experiment (the resolution of the TB-LMTO recursion may be estimated to be 0.05 to 0.1 eV, depending on the number of recursion levels and the order of the approximant), but not for exploring transport properties depending on the DOS in a very narrow interval around E_F and on the character of the eigenstates (which cannot be characterized by recursion calculations on models with moderate linear dimension).

4.2. Electronic spectrum of higher-order approximants

Figure 5 shows the electronic density of states for 3/2-, 5/3- and 8/5-approximants to the icosahedral phase, calculated on the basis of canonical cell tilings with the atomic coordinates relaxed under the constraint of conserving the symmetry of the approximant. Out of the possible models within each class of approximants we have chosen structures

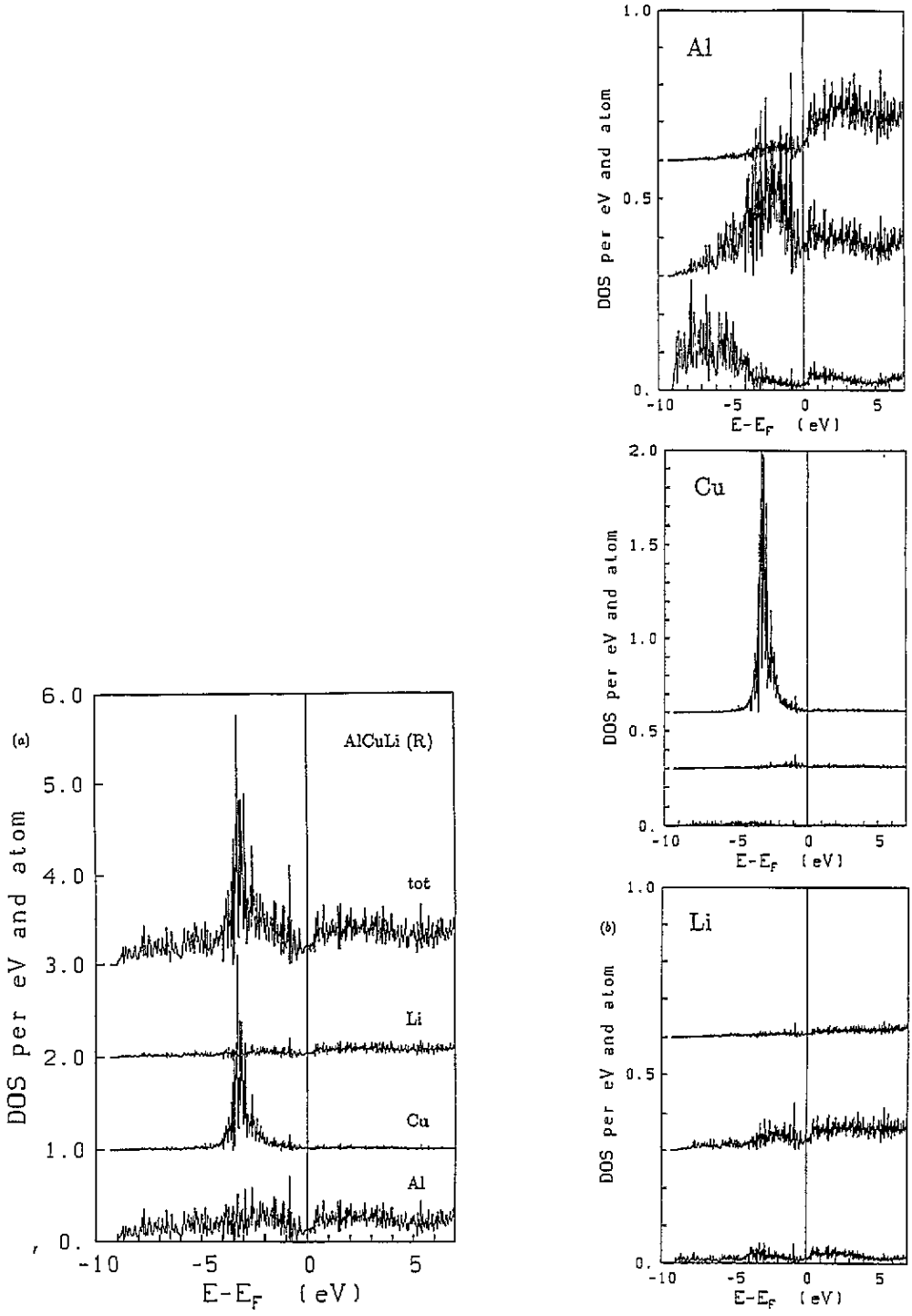

Figure 2. Total and local densities of states for R-phase AlCuLi (*a*), calculated using the self-consistent LMTO-method in *k*-space. The individual curves have been displaced vertically by one unit for clarity. Part (*b*) shows the angular-momentum decomposed DOSs, in the sequence s, p, d from bottom to top. For clarity the individual curves have been dispaced vertically by 0.1 states per eV and atom.

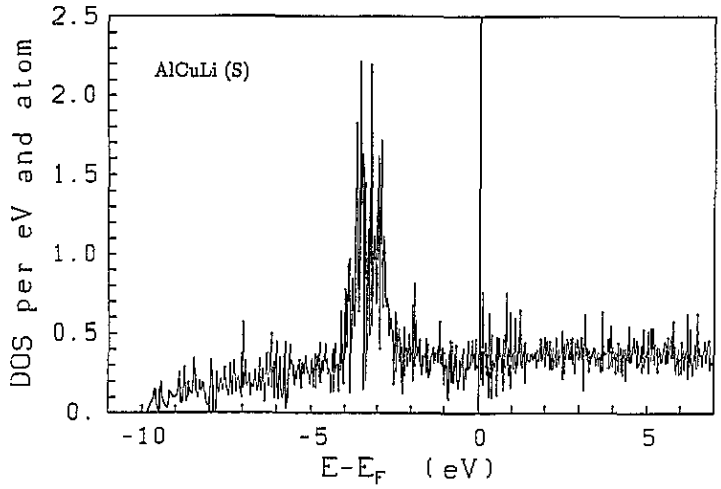

Figure 3. Total density of states for a symmetric *1/1*-approximant to *i-AlCuLi* (corresponding to a shifted acceptance domain).

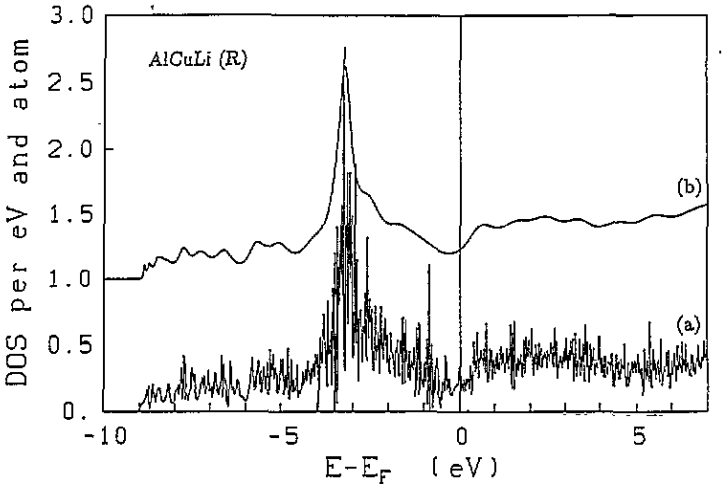

Figure 4. Comparison of the densities of states for R-phase AlCuLi as calculated with the *k-space* LMTO *technique* (bottom) and the real-space TB-LMTO recursion approach (top, displaced vertically by one unit).

which are most compact in perpendicular space. This would seem to guarantee that these models are also quite close to the models constructed by projection from the six-dimensional hypercubic lattice. These models contain 2888, 12 232 and 51 752 atoms in the periodically repeated cell. The calculations have been performed on the basis of a second-order TB-Hamiltonian (cf equation (2)) for each of the five topologically inequivalent sites (vertices, mid-edge positions, etc, occupied as in the R-phase). The self-consistent LMTO potential parameters resulting from the LMTO calculations for the 1/1-phase are used. The continued fraction for the DOS has been extended to 50 levels for the 3/2-, and 80 levels for the 5/3- and 8/5-approximants. Extension to 100 levels for the 8/5-approximant leaves the DOS

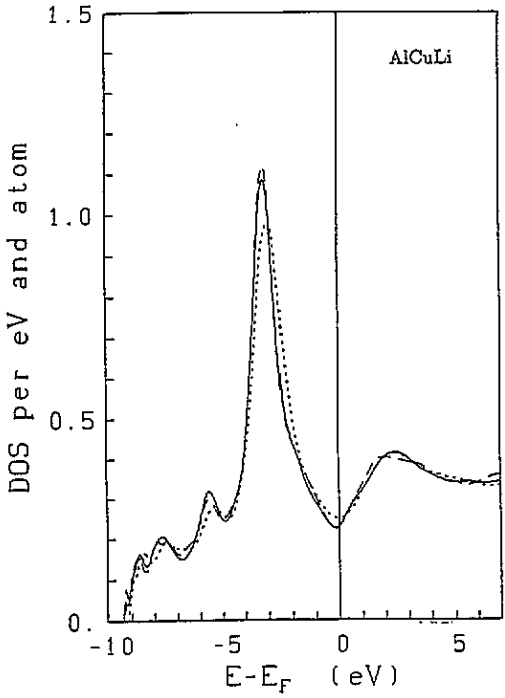

Figure 5. Electronic density of states for 3/2- (dotted curve), 5/3- (broken curve), and 8/5-approximants (full curve) to icosahedral AlCuLi, constructed in the canonical-cell-tiling model and relaxed under symmetry constraints.

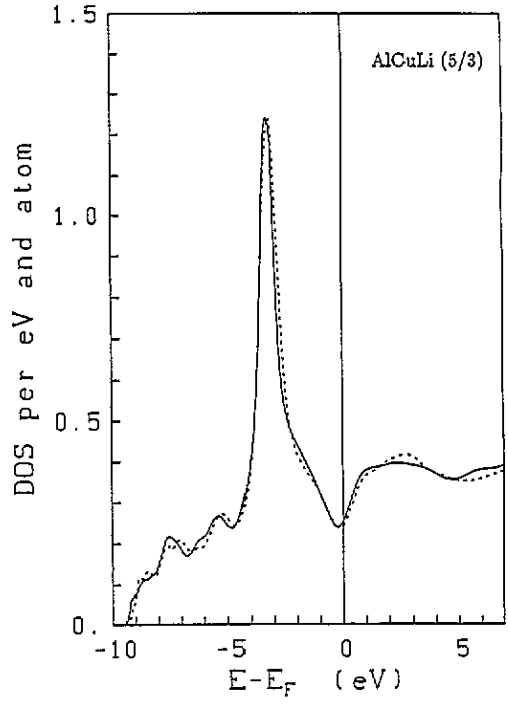

Figure 6. Comparison of the electronic density of states for 5/3-approximants of CCT (dotted curve) and 3DPT (full curve) models, free relaxation without symmetry constraints.

invariant.

The result shows very small changes in the electronic spectrum: at the Fermi level the DOS is $n(E_F)$=0.25, 0.22 and 0.22 states (eV atom)$^{-1}$ with increasing order of the approximants. This is in agreement with the nuclear magnetic resonance study of Hippert *et al* [26] who estimated a decrease of $n(E_F)$ of about 7% in the i-phase relative to the R-phase.

The result is not specific to the CCT models. This is demonstrated in figure 6 where we compare the DOS of the 5/3-approximants for the CCT and 3DPT models, with the atomic coordinates relaxed without any symmetry constraint. One remarkable difference is that the CCT models show more structure than the 3DPT models—a similar result has already been obtained for the phonon DOS [38]. It is related to the fact that the local structure is better defined in the CCT model: the idealized CCT model is less subject to a displacive modulation under the action of the interatomic forces. The effect of the relaxation is demonstrated in figure 7 where we compare the DOS for the 5/3-3DPT model in its idealized configuration and in two configurations relaxed with and without symmetry constraints. The fact that the displacive modulation induces only small changes in the electronic spectrum confirms that the modulation of the idealized quasicrystalline structure is sufficiently weak and does not affect the electronic factors favouring quasicrystalline stability in a negative way.

Finally, we have explored, in the example of the 5/3-approximant to the 3DPT, the effect of variations in the local chemical order on the electronic structure. The open question is

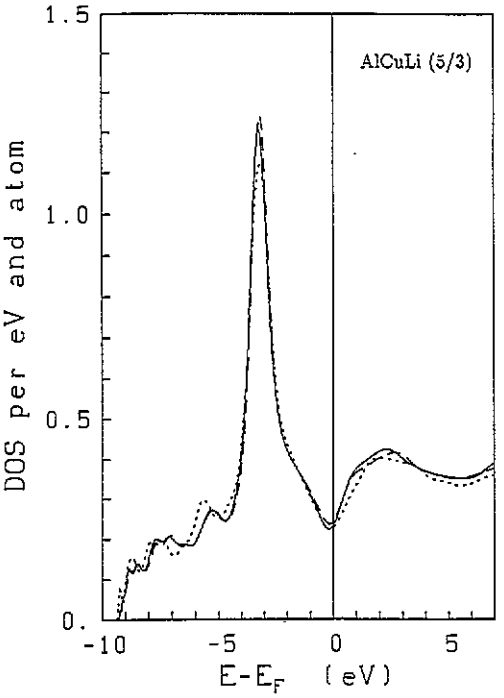

Figure 7. Comparison of the electronic density of states for CCT 5/3-approximants: idealized configuration (full curve), relaxed without symmetry constraints (broken curve), relaxed with symmetry constraints (dotted curve).

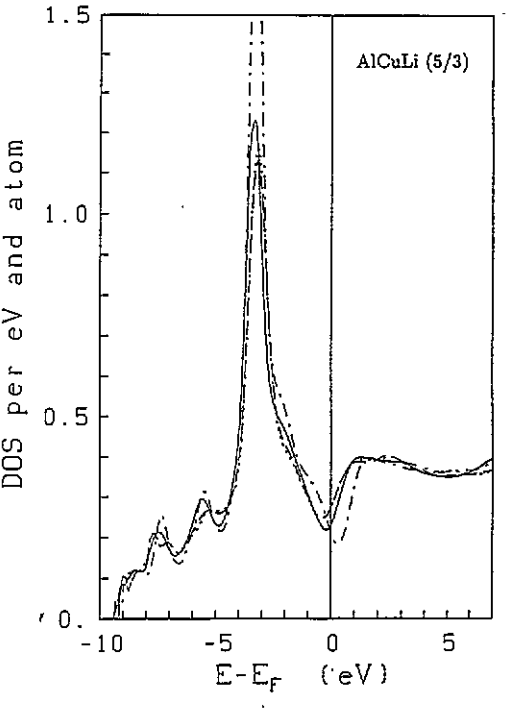

Figure 8. Effect of local chemical ordering on the electronic density of states of a 5/3-3DPT approximant to i-AlCuLi. The distribution of the Al and Cu atoms over the available sites is varied: (*a*) all vertices occupied by Cu (composition $Al_{52.73}Cu_{16.51}Li_{30.76}$, chain curve), (*b*) random occupation of vertices by Al and Cu, all mid-edge positions Al ($Al_{58.55}Cu_{10.69}Li_{30.36}$, full curve), (*c*) random distribution of Al and Cu over vertices and mid-edge positions ($Al_{57.59}Cu_{11.08}Li_{31.33}$, broken curve) and (*d*) random occupation mid-edge positions by Al and Cu, all vertices Al ($Al_{58.61}Cu_{10.63}Li_{30.76}$, dotted curve).

mainly the distribution of the Al (Cu) atoms over the vertex and mid-edge positions—the occupation of the remaining sites and the distribution of Al (Cu) against Li is fixed for steric reasons and the requirements of stoichiometry. Neutron scattering experiments [37, 54] with different Cu isotopes show little variation of the diffraction intensities, suggesting a random distribution of Al and Cu. On the other hand, refinement of single-grain diffraction data for CCT models shows that the crystallographic reliability factor (R-factor) measuring the mean-square deviations of the computed diffraction intensities from experiment may be lowered by assuming a larger percentage of Cu on the vertices (36% Cu) than on the mid-edge positions (12% Cu) [49]. Figure 8 shows a series of DOSs for the 5/3-3DPT approximant with varying distribution of Al and Cu: (*a*) all vertices occupied by Cu (this would increase the total Cu content to 16%, $Al_{52.73}Cu_{16.51}Li_{30.76}$), (*b*) random distribution of Cu on vertices, but respecting symmetry constraints ($Al_{58.55}Cu_{10.69}Li_{30.36}$), all mid-edge positions occupied by Al, (*c*) random distribution of Cu on vertex and mid-edge positions ($Al_{57.59}Cu_{11.08}Li_{31.33}$), and (*d*) random distribution of Cu on mid-edge positions ($Al_{58.61}Cu_{10.63}Li_{30.76}$), all vertices occupied by Al atoms. All configurations have been relaxed under symmetry constraints.

The change in the DOS is small—the most important effect is the change in the weight of the Cu-d band and the variation of the pseudogap as a consequence in the change of stoichiometry. Except for the case where all vertices are occupied by Cu atoms, the deepest pseudogap is found with a random occupation of the vertices of the rhombohedra by Al and Cu atoms, while all mid-edge positions are occupied by Al. This is in very good agreement with the result of the optimization of the R-factor predicting about 1:1 occupation for the vertices, but only 11% Cu on the mid-edge positions. The occupation of all vertices by Cu (leading to an even deeper pseudogap) gives a stoichiometry outside the observed range and some unfavourable short inter-atomic distances.

5. Band-gap creation in quasicrystals and approximants

The mechanics leading to the formation of pseudogaps in the electronic DOS of icosahedral quasicrystals has been addressed either (a) in a two-plane analysis based on the concept of the quasi-Brillouin zone [3–5] or (b) on the basis of the molecular eigenvalues of the icosahedral clusters existing in the quasilattice [55, 56]. The Brillouin zone is the polyhedron in reciprocal space formed by the planes bisecting the $\boldsymbol{Q}$ vectors belonging to the star of equivalent Bragg reflections. Interaction between the states at opposing faces of the Brillouin zone leads to the formation of gaps at certain $\boldsymbol{k}$-points, which upon $\boldsymbol{k}$-space integration become valleys in the electronic DOS. It has been argued [3–5, 11] that icosahedral symmetry leads to enhanced band-gap effects because of the high degeneracy of some stars of reciprocal lattice vectors. The variation of the band-gap effects in a hierarchy of approximants has been discussed by Carlsson [57].

Approach (b) concentrates on the local aspects of bonding in the distinctive icosahedral coordination environments of quasicrystals. It is argued that gaps exist in the local DOS of the icosahedral sites, whereas the non-icosahedral atoms do not show a gap in the local DOS at E_F and contribute to a background DOS of states in the icosahedral gap. To explain the increased stability of the icosahedral phase over the approximants, it is argued that the structural relaxation of the 'glue' atoms leads to the formation of a mini-gap via a Jahn–Teller-like mechanism [56]. This argument is certainly speculative to a large extent and in view of the very small number of glue atoms even in our largest model it is unlikely that the 'glue' pseudogap is really a decisive factor.

5.1. Reciprocal quasilattices

The disadvantage of the Brillouin-zone argument is that it is based on a rather sloppy application of the reciprocal space concept to quasicrystals. Niizeki [58, 59] was one of the first to show how these concepts may be extended to quasilattices: to the six-dimensional hypercubic lattice L_6 in the six-dimensional space E_6 there corresponds a six-dimensional reciprocal lattice L_6^* (again hypercubic) in the six-dimensional reciprocal space. A 6D Brillouin zone may be defined in the usual way, with special points of high symmetry: the Γ points at the centre of the zone, at the X_2, M_2, X_3, M_3, X_5, M_5 and the R points at the 'zone boundaries'. Representative wave vectors are (with $h = \frac{1}{2}$) (000000), (hh0000), (00$hhhh$), (hhh000), (000hhh), (h00000), (0$hhhhh$). The point group symmetry of the special points is the icosahedral group I_h for Γ and R, and D_{2h}, D_{3d} and D_{5d} for X and M, depending on whether the subscript is 2, 3 or 5. The projections of the 6D special points on 3D reciprocal space define sets of quasiperiodically distributed special points. The special points are dense everywhere, but with intensities modulated by interference effects and described by a generalized structure factor. Figure 1 just shows the intensities of the Γ points in a plane

containing the two-, three- and five-fold symmetry axes, calculated for the 5/3-approximant to the decorated 3DPT (within the accuracy of the graphical representation). Similar plots may be constructed for the other high-symmetry points. These quasiperiodically distributed sets of zone-centre (Γ) and the zone-boundary (X, M, R) points define the quasiperiodic analogue to the extended-zone scheme of a crystal (accounting for the modulation of the intensities arising from interference effects) and provide a solid basis for the extension of the band-gap concept to quasicrystals.

5.2. Quasiperiodic nearly-free-electron model

In the extended zone scheme of the nearly-free-electron model, each Γ point is the origin of a parabolic dispersion relation. In the case of a quasicrystal, there are free-electron parabolas everywhere, but their importance is weighted with the intensity of the corresponding Γ point. Figure 9 shows the intersection of the most intense free-electron parabolas with a plane passing through two two-fold symmetry axes: the parabolas having their origin at the bottom of the band are easily associated with the most intense Γ points situated along the two-fold axis (cf figure 1). The intersection of two or more free-electron parabolas defines a degenerate state whose degeneracy will be lifted through the interaction of the electron with the quasilattice, leading to the formation of a band gap at the particular $\boldsymbol{k}$ point whose width is proportional to the matrix element of the electron–ion pseudopotential and the structural weight of the Γ point at which the dispersion relation has its origin. Figure 9 also shows the position of some of the most intense X_2 and M_2 points. Note that in principle there will be gaps everywhere, but their contribution to the spectrum has to be weighted with the intensity of the corresponding Γ point.

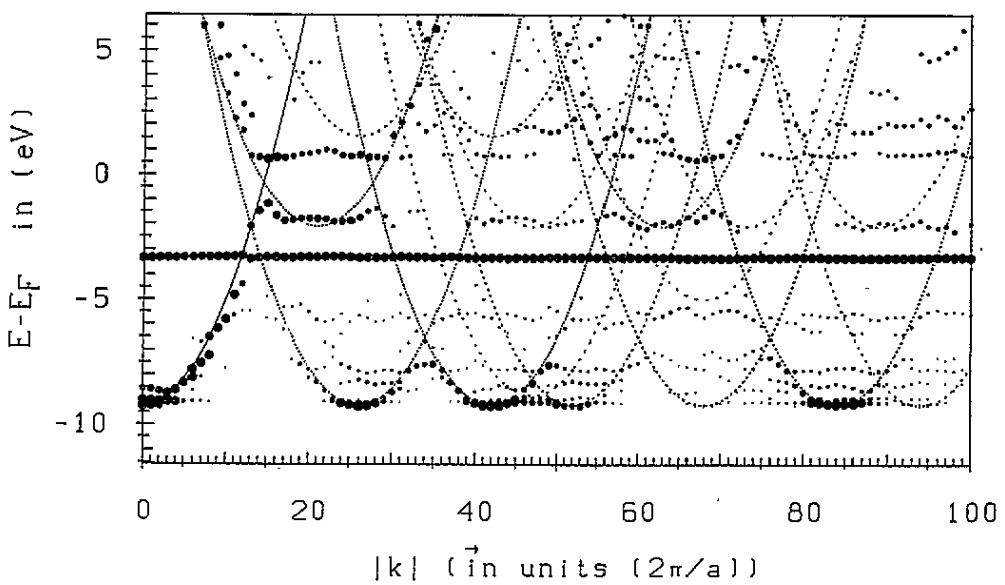

Figure 9. Dispersion relations $E(\boldsymbol{k})$ for electrons in the 5/3-approximant to icosahedral AlCuLi for $\boldsymbol{k}$-points along a twofold symmetry axis. Broken curves, free-electron parabolas originating from the most intense Γ points on and in the vicinity of the two-fold axis. Full points, dispersion relations as determined from the positions of the peaks in the Bloch spectral function $f(\boldsymbol{k}, E)$. The size of the dot scales with the amplitude of the peak. See text.

For AlCuLi, the degenerate free-electron states at binding energies of ~ -8.5, -6.5, -2 and 0 eV compare quite favourably with the minima in the calculated DOS, but the real task is to determine the dispersion relations of electrons in real quasicrystals.

5.3. Bloch spectral functions and dispersion relations for electrons in quasicrystals

In crystals the Bloch spectral function $f(\boldsymbol{k}, E)$ consists of a set of delta functions situated at the poles of the resolvent operator $(E - H)^{-1}$, their position in $\boldsymbol{k}$-space defining the dispersion relations (or band structure) of electrons in the crystal. For a quasicrystal, the delta-function poles are dense in $\boldsymbol{k}$-space and they are weighted by interference effects. The finite resolution of a recursion calculation produces a smooth Bloch spectral function whose peaks define the dispersion relations for the most important electron states in the quasicrystal.

Figure 10 shows the Bloch spectral function $f(\boldsymbol{k}, E)$ calculated using the recursion method for $\boldsymbol{k}$ vectors pointing along a two-fold axis, the maxima of this function defining the dispersion relations shown in figure 9. Similar results are obtained for all other high-symmetry directions. The most prominent peak in $f(\boldsymbol{k}, E)$ stems from the almost dispersion-less Cu-3d states, but the remaining states conform very well with the free-electron model (although the actual calculation has been performd within a tight-binding framework): one easily recognizes the nearly parabolic bands starting out from the most intense Γ points and the pseudogaps formed at the 'quasi-zone boundaries'. The coincidence of the Fermi level with a particular set of highly degenerate free-electron states depends on the filling of the band and hence on the electron/atom ratio. This completes the analogy with the crystalline and amorphous Hume–Rothery phases [13–16].

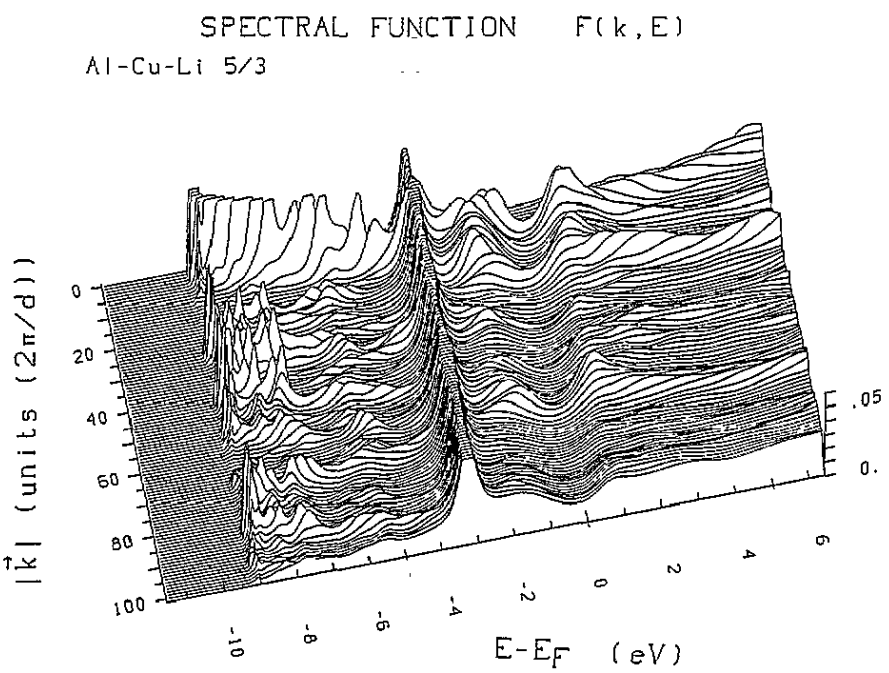

Figure 10. Bloch spectral function $f(\boldsymbol{k}, E)$ for electrons in the 5/3-approximant to icosahedral AlCuLi with $\boldsymbol{k}$ pointing along a two-fold symmetry direction.

It is important that the same arguments apply to other elementary excitations in quasicrystals, e.g. phonons [38, 60, 61]. The Γ points are the origin of the dispersion relations (linear for phonons) of propagating eigenstates, and the lifting of their degeneracy leads to a stationary-mode behaviour at the 'quasi-zone boundary'. For phonons, this scenario given on the basis of theoretical arguments is confirmed by inelastic neutron scattering experiments [62, 63].

5.4. Band-gap formation

The mechanism for band-gap creation discussed in the previous section differs significantly from pseudo-Brillouin-zone arguments discussed in the literature [4, 5, 11]. There, very much in the spirit of a reduced-zone picture, the argument was based on a single Brillouin zone (that corresponding to the (111101) point in the case of i-AlCuLi and i-AlZnMg) making contact with the free-electron Fermi sphere. These considerations stress the importance of the icosahedral point-group symmetry, but largely ignore the aspect of quasiperiodicity. The important consequence of quasiperiodicity is that the Γ points are dense everywhere in $\boldsymbol{k}$-space with a quasiperiodic modulation of their intensities. This leads to quasiperiodic free-electron dispersion curves and a quasiperiodic sequence of highly degenerate free-electron states. The lifting of the degeneracy of these states leads to the formation of a pseudogap, not only at an isolated $\boldsymbol{k}$ point, but extending throughout $\boldsymbol{k}$-space (see figure 10) at a constant energy.

The fact that the electron states close to the Fermi energy are stationary is also important in understanding the anomalous transport properties: not only does the reduced DOS at the Fermi edge lead to an increased resistivity, but the stationary character of the electron states also leads to a low Fermi velocity and hence to a further reduction of the conductivity.

6. Comparison with experiment

We have already mentioned that the calculated DOS at E_F agrees well with the data extracted from the electronic specific. More information on the valence-band spectrum may be obtained from soft x-ray emission (SXS) [22] and photoemission spectroscopy (PES) [64]. Figure 11 compares the calculated Al s+d DOS for the 1/1- and 5/3-approximants with the measured Al-$L_{2,3}$ SXS spectra of the R- and i-phases of AlCuLi and of pure FCC Al. The absence of the threshold singularity characteristic of the pure simple metals [65] is common to the calculated and measured spectra of the R- and i-phases; it confirms the predicted reduction of the DOS at the Fermi level. However, we note that the pseudogap is most pronounced in the Al-p partial DOS, so that the Al-K_β spectrum would be more informative than the L spectrum. The broad peak at a binding energy of about 5.5 eV arises mainly from the s states. The structure in the calculated spectrum is reflected in the asymmetry of the measured intensity. Figure 12 shows the Li-K_β spectrum for the pure metal and the R- and i-phases, compared with the partial Li-p DOS. Again, the marked peak at the threshold of the spectrum of the pure metal is replaced by a rounded peak in both the R- and i-phases. Agreement between theory and experiment is good when we match the maxima of the spectra, as far as the shape and width of the spectrum are concerned. At the Fermi level, the computation predicts a somewhat higher Li-p partial DOS than is observed in experiment. The shape of the experimental curve at E_F, however, looks curious (no sharp Fermi cut-off) and deserves re-investigation.

The photoemission spectrum results, to a first approximation, an average over the local partial densities of states, weighted with the partial photoionization cross sections

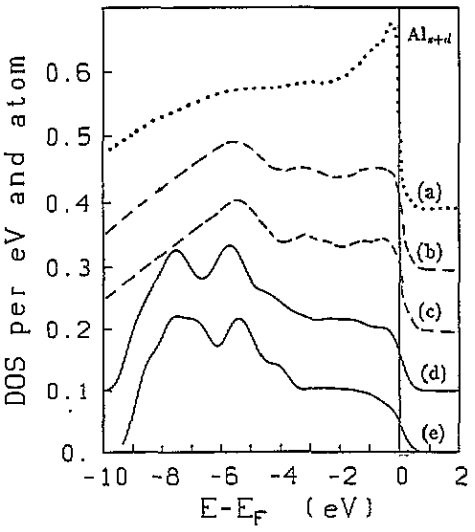

Figure 11. Al s+d partial densities of states (full curves) compared to the Al-$L_{2,3}$ SXS spectrum (after [22], broken curves), in the R-phase (c, e) and QC-phases (b, d) of AlCuLi. The spectrum for pure Al is shown for comparison (a). Each successive curve is displaced vertically by 0.1 units.

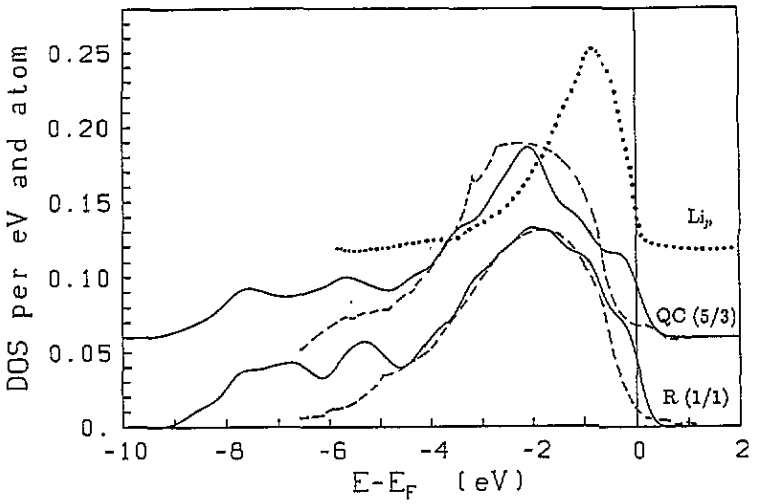

Figure 12. Li-p partial density of states (full curves) compared to the Li-K_β SXS spectrum (broken curves, after [22]), in the R- and QC-phases of AlCuLi. The spectrum for pure Li is shown for comparison (dotted curve). For each set of data, the zero of the DOS has been shifted vertically by 0.06 DOS units.

$\sigma_{i,l}(E, h\nu)$. At sufficiently high photon energies (i.e. in the X-ray PES regime), the cross section may be calculated as a function of the electron binding energy E in a single-scatterer final-state approximation [66, 67]. The available experimental data have been taken at photon energies of $\hbar\omega = 100$ and $\hbar\omega = 40$ eV. At least for the lower energy, we must admit that it is perhaps no longer admissible to neglect k-vector conservation, although the k vector is not a good quantum number for quasicrystals. An in depth discussion of the photoemission process in quasicrystals, however, would lead too far in the present context. A further problem arises from the fact that for the narrow Cu-d band self-interaction

corrections for the Cu-d hole lead to an apparent [14, 68] shift of the d-band by about 1 eV to larger binding energies. Figure 13 shows the calculated PES intensities for the 5/3-CCT model compared with experiment. The position of the Cu-d DOS has been shifted so as to match the experiment (simulating the effect of the self-energy of the d-band hole). We find reasonable agreement between theory and experiment, in particular concerning the existence of a reduced DOS at E_F which is more distinctly visible in the 100 eV spectra.

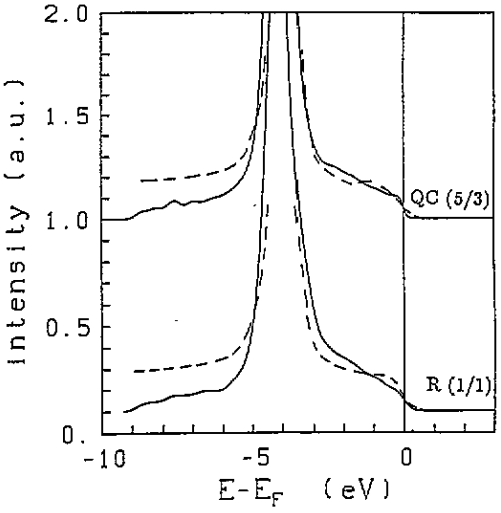

Figure 13. PES spectrum ($h\nu$ = 100 eV) for R- and QC-phase AlCuLi, calculated with shifted Cu-d band (full curves). Experimental spectra [22] are shown by the broken curves, cf text. For the PES spectrum of the quasicrystal, the zero of the intensity has been shifted vertically by one unit.

7. Conclusions

We have presented detailed results on the electronic spectrum of a hierarchy of approximant crystals to icosahedral quasicrystals in the AlCuLi system. We have shown that the pseudogap at the Fermi energy is a generic, structure-induced feature of the entire hierarchy of approximants (our calculations extend up to the 8/5-approximant with more than 55 000 atoms in the periodically repeated cell), and hence also of the quasicrystal. The existence of the pseudogap is not greatly sensitive to details of the structural model: it exists in Penrose tiling as well as in canonical cell tiling models (this shows that the existence of large icosahedral clusters is not a condition for the formation of the pseudogap, since these clusters exist in the CCT, but not necessarily in the larger 3DPT approximants). It is also compatible with a certain degree of chemical disorder. The depth of the pseudogap varies only insignificantly in the hierarchy of the approximants—this is in agreement with the available spectroscopic data [22, 26, 64] and is reasonable from the point of view of energetics since for AlCuLi both the 1/1-approximant and the quasicrystal are thermodynamically stable. Evidently this is possible only if they receive a comparable pseudogap stabilization.

Acknowledgments

This work has been supported by the Austrian Science Foundation under project no P9678-PHYS. The cooperation of Dr M Mihalkovič who constructed the canonical cell models is gratefully acknowledged.

References

[1] Shechtmann D, Blech I, Gratias D and Cahn J W 1984 *Phys. Rev. Lett.* **53** 1951
[2] Bancel D A and Heiney P A 1986 *Phys. Rev.* **33** 7917
[3] Smith A P and Ashcroft N W 1987 *Phys. Rev. Lett.* **59** 1356
[4] Vaks V G, Kamyshenko V V and Samolyuk G D 1988 *Phys. Lett.* A **132** 131
[5] Friedel J 1988 *Helv. Phys. Acta* **61** 538
[6] Tsai A P, Inoue A and Masumoto T 1991 *Sci. Rep. Res. Inst. Tohoku Univ.* A **36** 112
[7] Biggs B D, Poon S J and Munirathnam N R 1990 *Phys. Rev. Lett.* **65** 2700
[8] Pierce F S, Poon S J and Biggs B D 1993 *Phys. Rev. Lett.* **70** 3919
[9] Kimura K, Iwahashi H, Hashimoto T, Takeuchi S, Mizutani U, Ohashi S and Itoh G 1989 *J. Phys. Soc. Japan* **58** 2472
[10] Mizutani U 1988 *Mat. Sci. Eng.* **99** 165
[11] Poon S J 1992 *Adv. Phys.* **41** 303
[12] Nagel S R and Tauc J 1975 *Phys. Rev. Lett.* **35** 380
[13] Hafner J and von Heimendahl L 1980 *Phys. Rev. Lett.* **42** 385
[14] Hafner J, Jaswal S S, Tegze M, Pflugi A, Oelhafen P and Güntherodt H J 1988 *J. Phys. F: Met. Phys.* **18** 2583
[15] Häussler P 1992 *Phys. Rep.* **222** 65
[16] Mizutani U and Massalski T B 1978 *Prog. Mater. Sci.* **22** 152
[17] Hafner J 1989 *The Structures of Binary Compounds* ed F R de Boer and D G Pettifor (Amsterdam: North-Holland) ch 3 §6.2
[18] Bergman G, Waugh J T and Pauling L 1957 *Acta Crystallogr.* **10** 147
[19] Henley C L and Elser V 1986 *Phil. Mag.* B **53** L59
[20] Guryan C A, Stephens P W, Goldman A I and Gayle F W 1988 *Phys. Rev.* B **37** 8495
[21] Mukhopadhyay N K, Ishihara K N, Ranaganathan S and Chattopadhyay K 1991 *Acta Metall.* **39** 1151
[22] Bruhwiler A, Wagner J L, Biggs B D, Shen Y, Wong K M, Schnatterly S E and Poon S J 1988 *Phys. Rev.* B **33** 6529
[23] Belin E and Traverse A 1991 *J. Phys.: Condens. Matter* **3** 2157
[24] Belin E, Dankhazi Z, Sadoc A, Calvayrac Y, Klein T and Dubois J M 1992 *J. Phys.: Condens. Matter* **4** 4459
[25] Mori M, Matsuo S, Ishimasa T, Matsuura T, Kamiya K, Inokuchi H and Matukawa 1991 *J. Phys.: Condens. Matter* **3** 767
[26] Hippert F, Kandel L, Calvayrac Y and Dubost B 1992 *Phys. Rev. Lett.* **69** 2086
[27] Matsubara H, Ogawa S, Kinoshita T, Takeuchi S, Kimura K and Suga S 1991 *Jpn. J. Appl. Phys.* **30** L389
[28] Wagner J L, Biggs B D, Wong K M and Poon S J 1988 *Phys. Rev.* **38** 7436
[29] Fujiwara T and Yokokawa T 1992 *Phys. Rev. Lett.* **66** 333
[30] Fujiwara T 1989 *Phys. Rev.* **40** 952
[31] Hafner J and Krajčí M 1992 *Europhys. Lett.* **17** 145
[32] Hafner J and Krajčí M 1992 *Phys. Rev. Lett.* **62** 2321
[33] Hafner J and Krajčí M 1993 *Phys. Rev.* B **47** 11795
[34] Mukhopadhyay N K, Isihara K N, Ranagathan S and Chattopadhyay L 1991 *Acta Metall.* **39** 1151
[35] Krajčí M and Hafner J 1992 *Phys. Rev.* B **46** 10669
[36] Henley C L and Elser V 1986 *Phil. Mag. Lett.* **53** 115
[37] de Boissieu M, Janot C, Dubois J M, Audier M, Jaric M and Dubost B 1990 *Quasicrystals* ed M V Jaric and S Lundqvist (Singapore: World Scientific) p. 109
[38] Windisch M, Hafner J, Krajčí M and Mihalkovič M 1994 *Phys. Rev.* B at press
[39] Henley C L 1991 *Phys. Rev.* B **43** 993
[40] Mihalkovič M and Mrafko P 1993 *J. Non-cryst. Solids* **156–8** 936
[41] de Boissieu M, Janot C, Dubois J M, Audier M and Dubost B 1991 *J. Phys.: Condens. Matter* **3** 1
[42] Skriver H L 1984 *The LMTO Method* (Berlin: Springer)
[43] Andersen O K, Jepsen D and Šob M 1987 *Electronic Band Structure and its Applications* ed M Yossouff (Berlin: Springer)
[44] Bose S K, Jaswal S S, Andersen O K and Hafner J 1988 *Phys. Rev.* B **37** 9955
[45] Heine V, Bullet D, Haydock R and Kelly M J 1980 *Solid State Physics* ed H Ehrenreich, D Turnbull and F Seitz (New York: Academic) vol. 35
[46] Audier M and Guyot P 1990 *Quasicrystals and Incommensurate Structures in Condensed Matter* ed M J Jacaman, D Romeu, V Castano and A Gomez (Singapore: World Scientific) p 181
[47] Elser V 1986 *Acta Crystallogr.* A **42** 36

[48] Newman M and Henley C L 1993 *J. Non-Cryst. Solids* **153–4**
[49] Mihalkovič M and Mrafko P 1994 *Phil. Mag. Lett.* **69** 85
[50] Hafner J 1983 *Phys. Rev.* B **27** 678
[51] Nex C M M 1978 *J. Phys. A: Math. Gen.* **11** 653
[52] Luccini M U and Nex C M M 1987 *J. Phys. C: Solid State Phys.* **20** 3125
[53] Fujiwara T and Yokokawa T 1990 *Quasicrystals* ed T Fujiwara and T Ogawa (Berlin: Springer)
[54] Janot C, de Boissieu M, Dubois J M and Pannetier J 1989 *J. Phys.: Condens. Matter* **1** 1029
[55] Hatakeyama T and Kamimura H 1992 *Solid State Commun.* **84** 227
[56] Phillips J C 1993 *Phys. Rev.* B **47** 2522
[57] Carlsson A E 1993 *Phys. Rev.* B **47** 2515
[58] Niizeki K 1989 *J. Phys. A: Math. Gen.* **22** 4295
[59] Niizeki K and Akamatsu T 1990 *J. Phys.: Condens. Matter* **2** 2759
[60] Hafner J and Krajčí M 1993 *J. Phys.: Condens. Matter* **5** 2489
[61] Pateł H and Sherrington D 1989 *Phys. Rev.* B **40** 11 185
[62] Goldman A I, Stassis C, Bellisent R, Moudden H, Pyka N and Gayle F W 1991 *Phys. Rev.* B **43** 8736
[63] Goldman A I, Stassis C, de Boissieu M, Currat R, Janot C, Bellisent R, Moudden H and Gayle F W 1992 *Phys. Rev.* B **45** 10 280
[64] Matsubara H, Ogawa S, Kinoshita T, Kishi K, Takeuchi S, Kimura K and Suga S 1991 *Jpn. J. Appl. Phys.* **30** L389
[65] Citrin P H, Wertheim G K and Schlüter M 1979 *Phys. Rev.* B **20** 3067
[66] Marksteiner P, Redinger J and Weinberger P 1986 *Z. Phys* B **63** 321
[67] Jank W and Hafner J 1990 *J. Phys.: Condens. Matter* **2** 5065
[68] Himpsel F J, Eastman D E, Koch E E and Williams A R 1980 *Phys. Rev.* B **22** 4604